AD-A067 257 SACLANT ASW RESEARCH CENTRE LA SPEZIA (ITALY) F/G 20/1
OBSERVED SOUND-SPEED VARIABILITY IN THE GULF OF CADIZ.(U)
FEB 79 J CAIRNS, L TOMA

UNCLASSIFIED SACLANTCEN-SM-122 NL

| OF |
AD
A067257

END
DATE
FILMED
6 --79
DDC

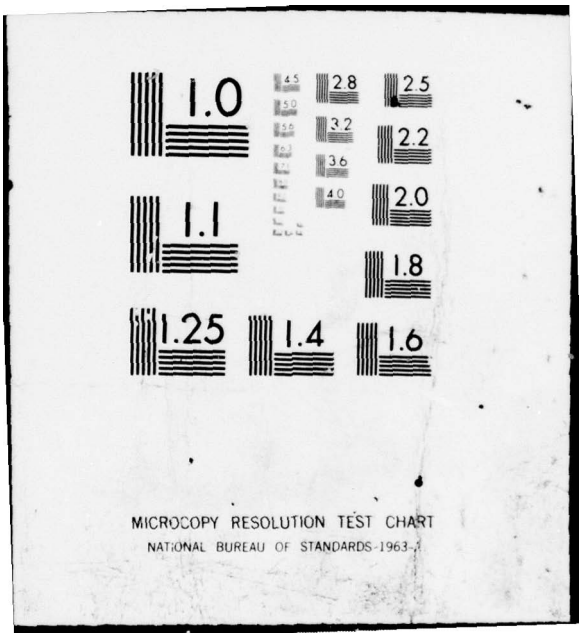
1.0
1.1
1.25
1.4
1.6
1.8
2.0
2.2
2.5
2.8
3.2
3.6
4.0
4.5
5.0
5.6
MICROCOPY RESOLUTION TEST CHART
NATIONAL BUREAU OF STANDARDS-1963-A

SACLANTCEN Memorandum SM-122

AD A067257

DDC FILE COPY

SACLANTCEN Memorandum SM-122

LEVEL II

SACLANT ASW RESEARCH CENTRE MEMORANDUM

OBSERVED SOUND-SPEED VARIABILITY IN THE GULF OF CADIZ

by

JAMES CAIRNS and LUCIO TOMA

Memorandum rept.,

1 FEBRUARY 1979

23 p.

NORTH ATLANTIC TREATY ORGANIZATION

LA SPEZIA, ITALY

Published by

SACLANTCEN

INITIAL DISTRIBUTION

MINISTRIES OF DEFENCE	Copies
MOD Belgium	2
DND Canada	10
CHOD Denmark	8
MOD France	8
MOD Germany	15
MOD Greece	11
MOD Italy	10
MOD Netherlands	12
CHOD Norway	10
MOD Portugal	5
MOD Turkey	5
MOD U.K.	16
SECDEF U.S.	61

NATO AUTHORITIES	
Defence Planning Committee	3
NAMILCOM	2
SACLANT	10
SACLANTREPEUR	1
CINCWESTLANT/COMOCEANLANT	1
COMIBERLANT	1
CINCEASTLANT	1
COMSUBACLANT	1
COMMAIREASTLANT	1
SACEUR	2
CINCNORTH	1
CINCSOUTH	1
COMNAVSOUTH	1
COMSTRIKFORSOUTH	1
COMEDCENT	1
COMMARAIRMED	1
CINCHAN	1

SCNR FOR SACLANTCEN	Copies
SCNR Belgium	1
SCNR Canada	1
SCNR Denmark	1
SCNR Germany	1
SCNR Greece	1
SCNR Italy	1
SCNR Netherlands	1
SCNR Norway	1
SCNR Portugal	1
SCNR Turkey	1
SCNR U.K.	1
SCNR U.S.	2
SECGEN Rep.	1
NAMILCOM Rep.	1

NATIONAL LIAISON OFFICERS	
NLO Canada	1
NLO Denmark	1
NLO Germany	1
NLO Italy	1
NLO U.K.	1
NLO U.S.	1

NLR TO SACLANT	
NLR Belgium	1
NLR Canada	1
NLR Germany	1
NLR Greece	1
NLR Italy	1
NLR Norway	1
NLR Portugal	1
NLR Turkey	1

Total initial distribution	232
SACLANTCEN STI Library	10
SACLANTCEN STI Stock	38
Total number of copies	280

(12)

SACLANTCEN MEMORADUM SM-122

NORTH ATLANTIC TREATY ORGANIZATION

SACLANT ASW Research Centre
Viale San Bartolomeo 400, I-19026 San Bartolomeo (SP), Italy.

tel: national 0187 503540
international + 39 187 503540

telex: 271148 SACENT I

OBSERVED SOUND-SPEED VARIABILITY IN THE GULF OF CADIZ

by

James Cairns and Lucio Toma

1 February 1979

This memorandum has been prepared within the SACLANTCEN Underwater Research Division.

G.C. VETTORI
Division Chief

TABLE OF CONTENTS

		Pages
ABSTRACT		1
INTRODUCTION		5
1	THE EXPERIMENT	5
	1.1 Data	7
2	SEPARATION OF EFFECTS	11
3	ANALYSIS AND RESULTS	13
	3.1 The Spectra	13
	3.2 Model Comparison	16
	3.3 Coherence Scales	17
	3.4 The Nearshore Region	18
CONCLUSIONS		18
AKCNOWLEDGMENTS		20
REFERENCES		20
APPENDIX A		21

List of Figures

1.	A sketch of towed oscillating body (TOB) showing path in space	6
2.	Area of experiment, showing ship's tracks	8
3.	Sound-speed profile derived from a CTD cast taken at the end of tow segment 5	8
4.	Sequential profiles of potential temperature, salinity, sound speed, and potential density along a section of tow segment 8	9
5.	Sequential profiles of potential temperature, salinity, sound speed, and potential density along a section of tow segment 4	10
6.	Examples of the fluctuations in sound speed	14
7.	Wavenumber spectra of the total fractional sound-speed fluctuations	15
8.	Spectrum of fractional sound speed fluctuations along tow track 8	19

OBSERVED SOUND-SPEED VARIABILITY IN THE GULF OF CADIZ

by

James Cairns and Lucio Toma

ABSTRACT

Sound-speed fluctuations have been examined by repeatedly profiling temperature, conductivity, and depth over long tow paths. The sound-speed variability due to internal waves conveniently separates from that due to inhomogeneities, revealing that even in an area of complex structure, internal waves are the leading cause of sound-speed fluctuations. At very low wavenumbers (<10^{-5} cycle/m), variability due to inhomogeneities nearly equalled that due to waves only, whereas at higher wavenumbers they contributed only about one fifth as much variability as waves. The Munk & Zachariasen model estimate of wave-induced fluctuations agrees very well with these data, and allows the further computation of local coherence lengths. A directional dependence of variability is found near the coast. Fluctuations were less by a factor of five looking along the coast than looking normal to it. It may be a general result that, in shoaling areas, sound-speed fluctuations measured parallel to the shore are less than those measured at right angles to the shore.

LIST OF UNDEFINED SYMBOLS

x,z	Horizontal, vertical coordinates
$(\hat{})$	Potential quantities referenced to sea's surface
k_H	Horizontal wavenumber
j	Internal wave mode number
B	Vertical scale length = 1000 m
ω_i	Inertial frequency = 0.05 cycle/h
$N(z),N_o$	Buoyancy frequency, surface extrapolated value
$\langle\ \rangle$	Mean value
rms ( )	Root of mean squared value
S,θ,ρ,P	Salinity (‰), Temperature (°C), Density (g/cm^3), Pressure
σ	= 1000 (ρ - 1.0)
a,b	Coefficients of thermal expansion and haline contraction
α,β,γ	$= C^{-1}\cdot(\frac{\partial}{\partial\theta}, \frac{\partial}{\partial S}, \frac{\partial}{\partial P})\ C$

INTRODUCTION

Variability of the oceanic structure on vertical scales of metres to tens of metres and horizontal scales of tens of metres to kilometres is dominated by two features. The structure is characterized by interleaving globs of diverse water types, which sort themselves out slowly under the influences of gravity, friction, and diffusion into a system of stable layers. They are evident as the steplike irregularities typically found in vertical profiles of the ocean's temperature and salinity. Additional variability arises from the continuous wobbling and straining of the whole layered system due to the action of internal waves. Both waves and globs contribute to irregularities in the sound field, and although their relative importance is not clear, internal waves are thought to be the dominant source of sound-speed fluctuations in the open sea *[1]*.

Differences in the way that waves and globs behave allow the separation of their effects. They are thought to have, first of all, very different time scales, globs persisting for times that are long compared with internal wave periods. Secondly, globs are characterized by a compensation of temperature and salinity that balances out horizontal irregularities in density (but not in sound speed), whereas internal waves have no such compensation. The purpose of the present study is to examine experimentally the separate contributions of globs and waves to fluctuations in the sound field.

Recently an experiment was staged in the oceanographically complex Gulf of Cadiz, where strong currents and waters of widely different origins exist in close proximity (See *[2]*, for example). One would therefore expect this to be an area where sound structure anomalies due to globs would be at their maximum. In spite of this, the sound-speed variance in the Gulf was found to be primarily due to internal waves.

1 THE EXPERIMENT

The experiment was conducted from SACLANTCEN's R/V MARIA PAOLINA G. in June 1977. Measurements were made with a towed sensor package (TOB) developed at SACLANTCEN *[3]*. The TOB instrumentation consisted of sensors and electronics from a Plessey model 9400 CTD modified to include a propeller-type current meter in a fourth channel*. It was mechanically designed for towing at modest speeds. A sketch of the TOB and its towing arrangement is shown in Fig. 1.

Data from the current meter are not discussed in this paper.

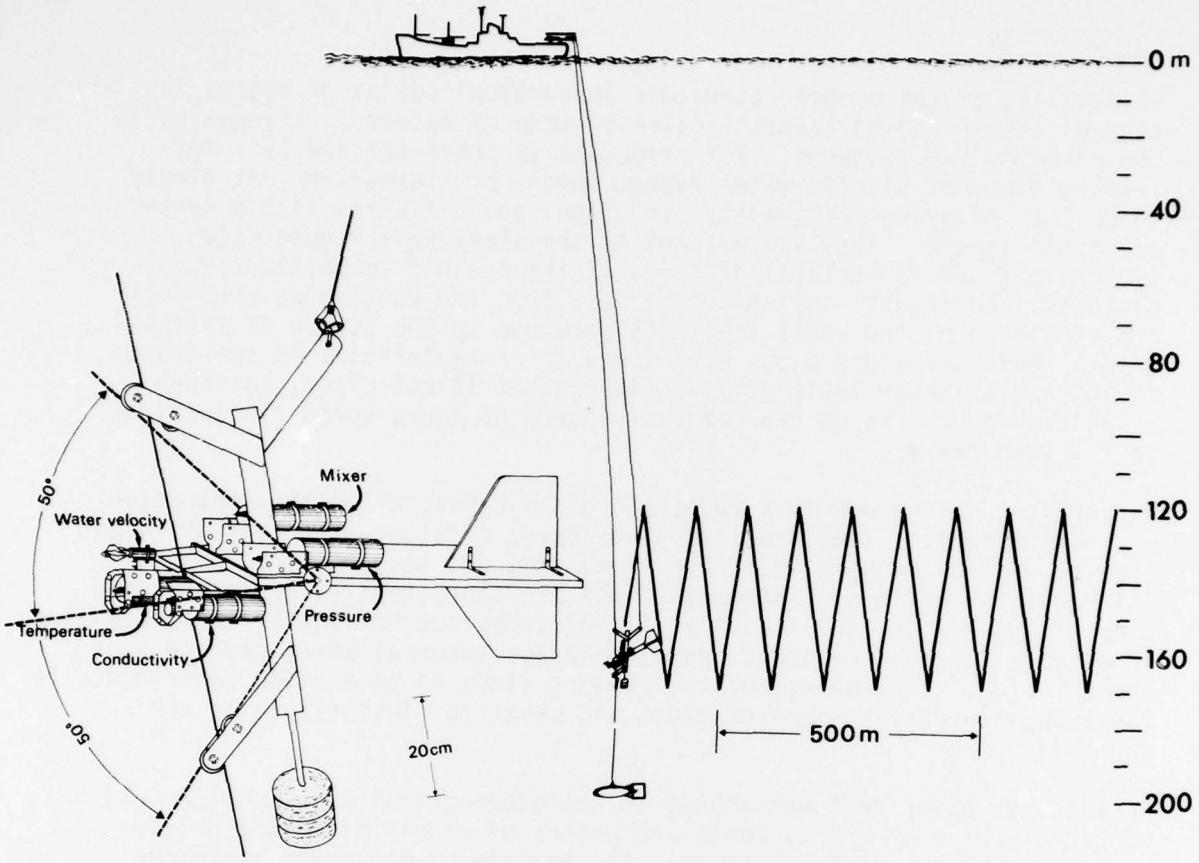

FIG. 1 A SKETCH OF THE TOWED OSCILLATING BODY (TOB) SHOWING PATH IN SPACE

While towed at 2 kn, the instrument package oscillated in depth along a taut cable between 120 m and 170 m. Average vertical sensor speed was 1 m/s; instantaneous speed varied somewhat due to the ship's pitching. The sensor path in space was nominally a 45° zig-zag line. Only the upward-travelling profiles were analyzed, giving on average a profile of 50 m vertical extent every 100 m along the ship's track. The routes along which the tows were made were determined by satellite navigation; they are shown in Fig. 2.

Temperature, conductivity, and pressure were simultaneously sampled 8 times per second and recorded as 16 bit binary coded numbers on magnetic tape. Their least count precisions are ±0.002°C, ±0.002 ms/cm*, and ±0.034 m (equivalent water depth), respectively. Time constants for the temperature, conductivity, and pressure probes are 0.4, 0.1, and 0.1 s respectively. The data were filtered to minimize the effects of the pitching ship, and time shifted to account for the diverse sensor time constants (see Appendix A).

1.1 Data

The data set is derived from about 350 km of tow and has been examined primarily for its sound-speed characteristics; a more detailed discussion of the physical structure of the water and its dynamics will be given in a separate paper *[4]*.

It is assumed throughout the discussion that the structure can be considered frozen in time, so that at a 2 kn tow speed only spatial changes are seen. This is thought to be a good assumption for the internal wave field *[5]*; it should be an even bettrr assumption for the glob field.

A profile in the upper kilometre (Fig. 3) gives an idea of the gross sound-speed structure. It was obtained from a deep CTD cast made at the end of tow segment 5.

The oceanic environment encountered along the tows ranged from very quiet areas, where both internal wave and glob activities were low, to regions of extreme structural convolutions with internal-wave levels typical of the open sea. Figure 4 shows a section of profiles demonstrating a quiet region along track 8. Each profile on the figure is a graph of one of the variables versus depth; successive profiles have been plotted by shifting the scale to the right by a fixed distance. On each profile the depths of encounter of particular values of the variables were registered. Lines passing from profile to profile through these depths give the changing elevation of the isopleths along the tow.

Figure 4 shows few inversions of the variables with depth, and the up and down oscillations of the iso-potential density surfaces (i.e. the internal waves) are small.

---

*The international unit, siemens (s), is equivalent to the previously-used mho.

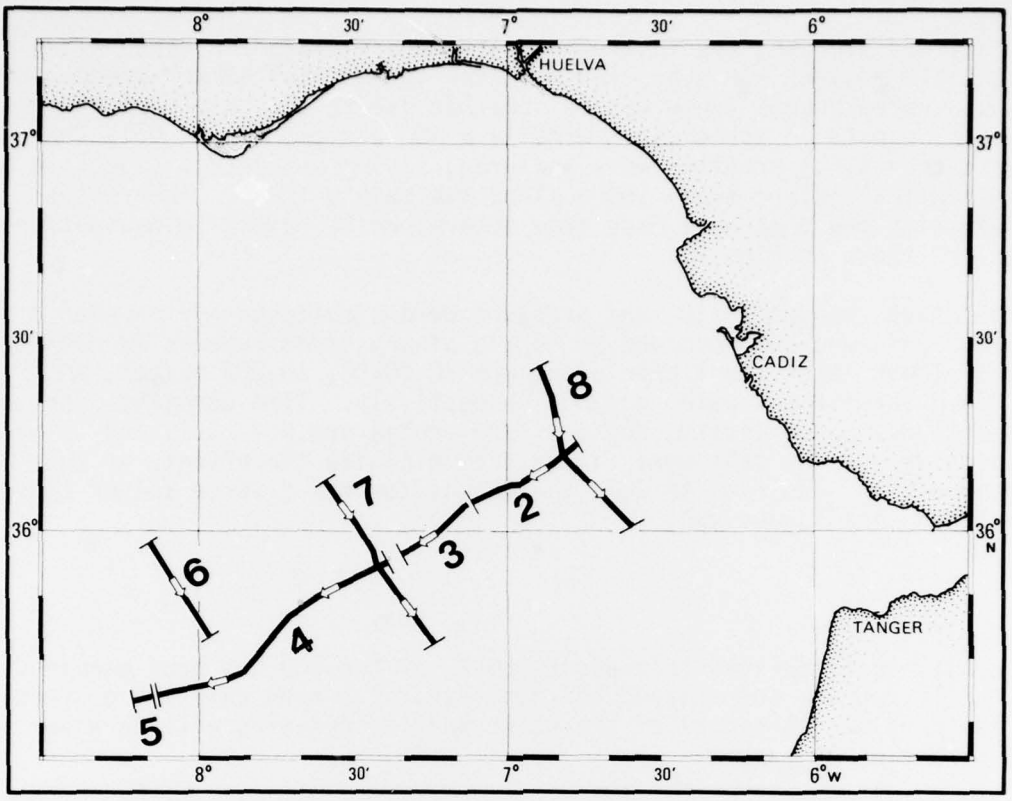

FIG. 2 AREA OF EXPERIMENT, SHOWING SHIP'S TRACKS

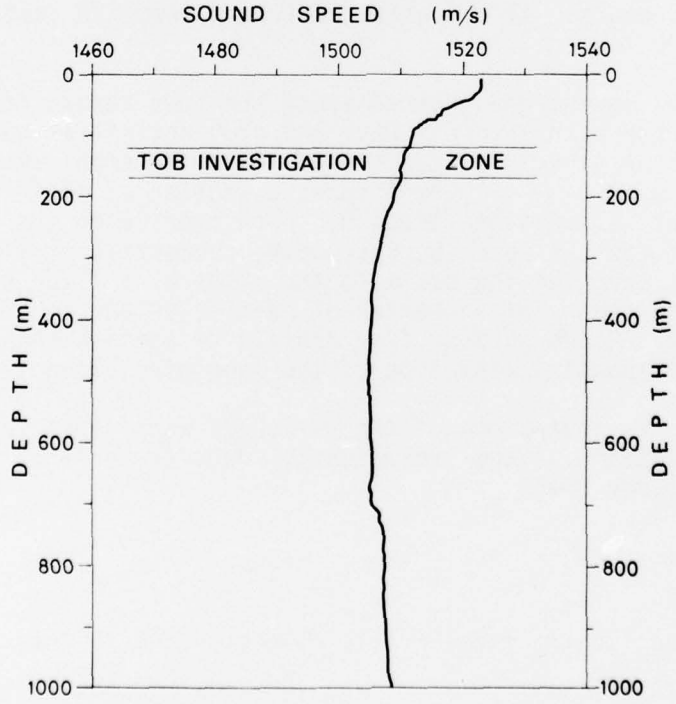

FIG. 3 SOUND-SPEED PROFILE DERIVED FROM A CTD CAST TAKEN AT THE END OF TOW SEGMENT 5

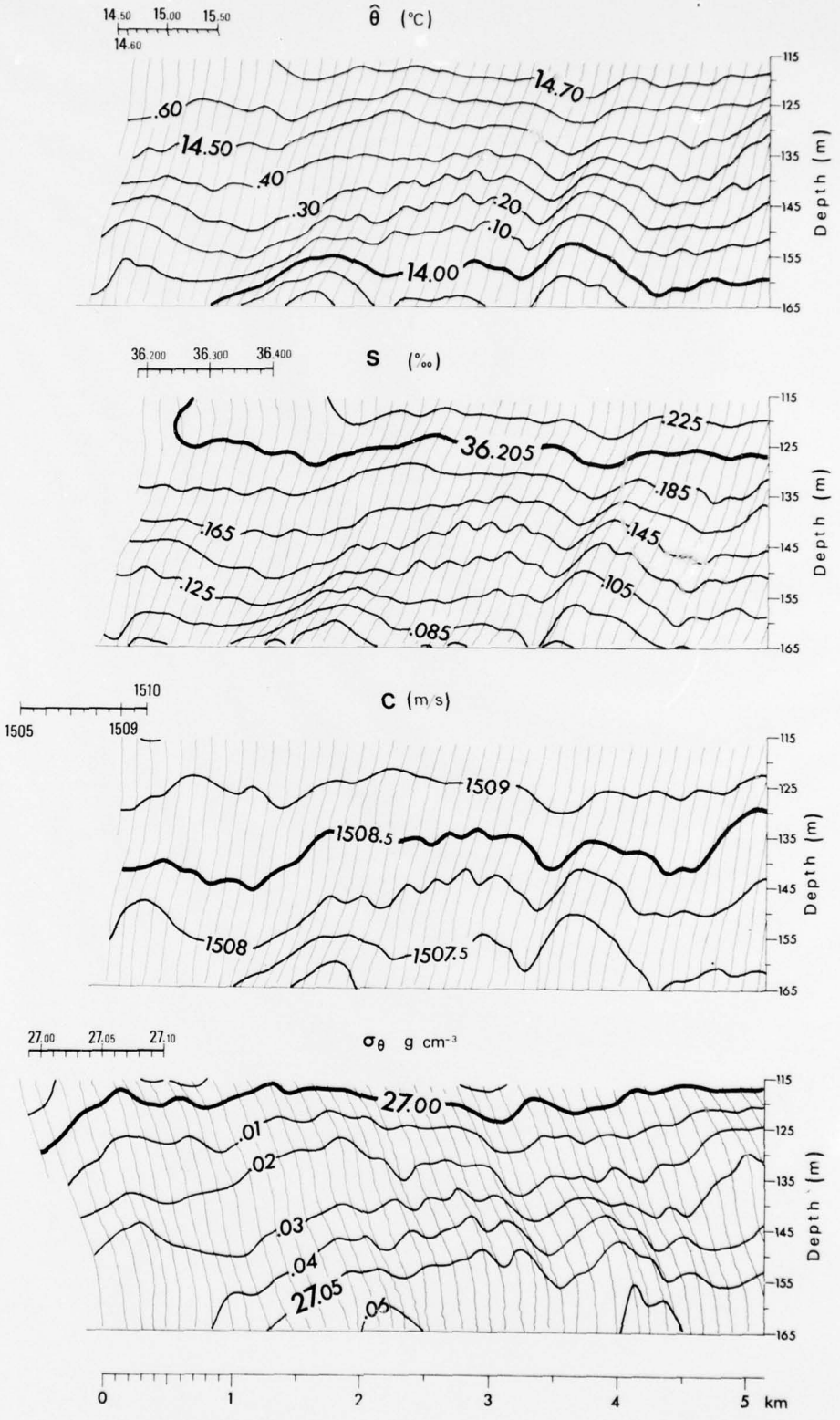

FIG. 4 SEQUENTIAL PROFILES OF POTENTIAL TEMPERATURE, SALINITY, SOUND SPEED, AND POTENTIAL DENSITY ALONG A SECTION OF TOW SEGMENT 8

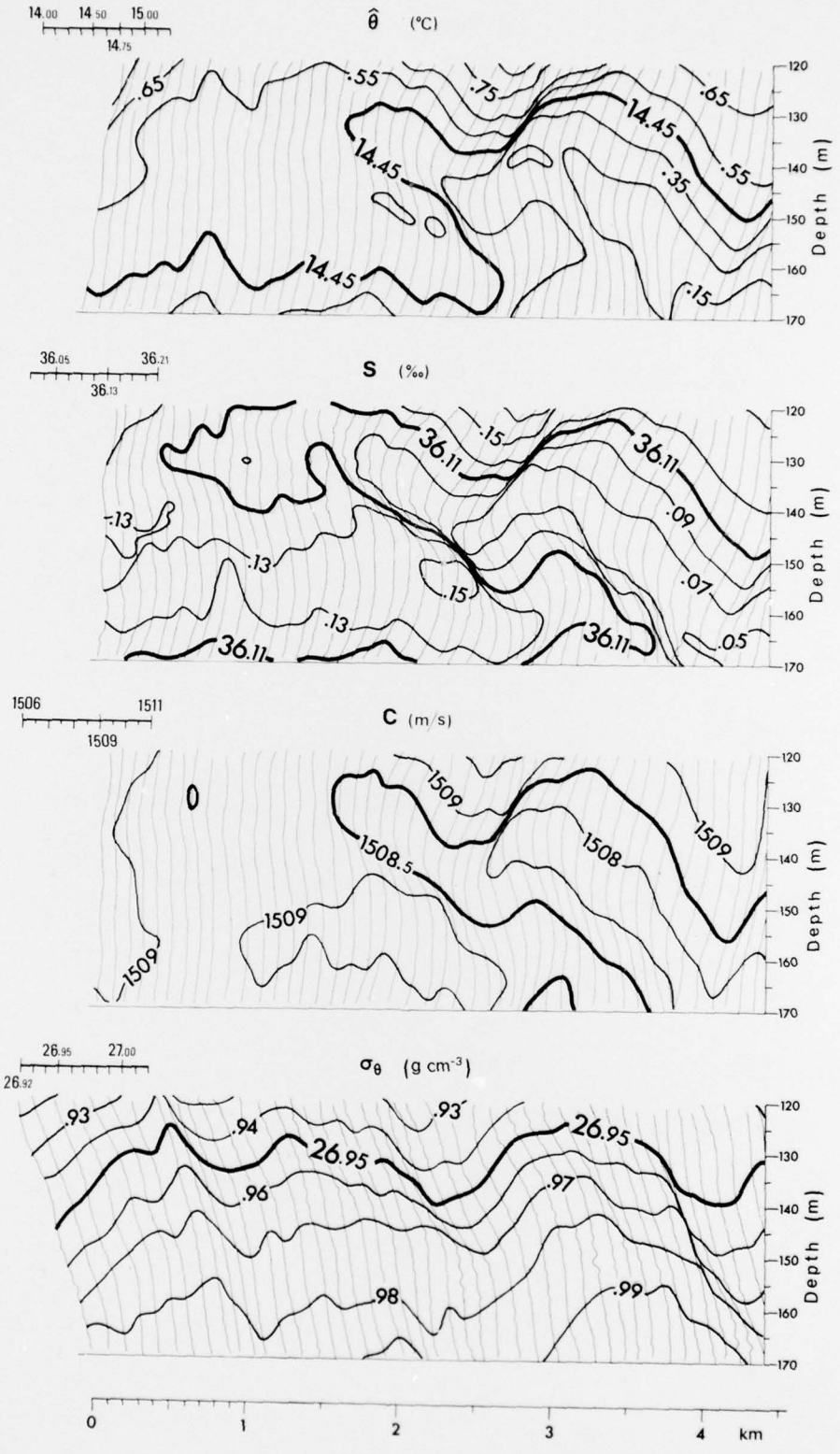

FIG. 5 SEQUENTIAL PROFILES OF POTENTIAL TEMPERATURE, SALINITY, SOUND SPEED, AND POTENTIAL DENSITY ALONG A SECTION OF TOW SEGMENT 4

In contrast, Fig. 5, from tow segment 4, depicts one of the most active regions. The fields of temperature, salinity, and sound speed appear to have been folded into complex patterns. Inversions in these fields were tens of metres high and several kilometres in horizontal extent. The potential density field on the other hand, which was presumably affected only by wave activity, showed no evidence of these distortions, although the wave activity itself was higher here than in the section shown in Fig. 4. Obviously in this area there was considerable variation of the sound speed due not directly to internal waves but to globs.

2 SEPARATION OF EFFECTS

As an aid to understanding sound-speed variability, the contribution due to internal waves was separated from that due to globs, using a scheme worked out in collaboration with Walter Munk of the Scripps Institution of Oceanography. The following discussion is limited to fluctuations along a horizontal path, as this is the only situation for which there were observations. We make the assumption that all the observed depth fluctuations of surfaces of constant potential density are due to internal waves.

It is useful to consider three cases.

Case 1 — waves only, no globs

In the presence of an internal wave field with displacement ζ, a particle momentarily at reference depth z_o has come from a rest position $z_o - \zeta$. The resulting sound speed at z_o is estimated to be

$$C(x,z_o) = C_o + \frac{\hat{dC}}{dz}\ \zeta(x), \qquad \text{[Eq. 1]}$$

where C_o is the average sound speed along $z = z_o$. Effects due to wave-induced particle velocities and pressure changes have been ignored, an approximation shown to be feasible by Munk & Zachariasen *[1]*.

To estimate the wave-induced variability from the data, where both waves and globs may be present, we write

$$C(x,z_o) = C_o + \overline{\frac{\hat{dC}}{dz}}\ (x)\ \zeta(x),$$

with $\overline{(\hat{dC/dz})}$ the local, average, vertical sound-speed gradient. For the wave-induced sound-speed fluctuation along z_o, this gives

$$\delta C_w(x,z_o) = \overline{(\frac{\hat{dC}}{dz})}\ (x)\ \zeta(x). \qquad \text{[Eq. 2]}$$

Case 2 — globs only, no waves

In the absence of motion, variability along a lateral path is due entirely to globs. Their contribution to the fluctuating sound speed in this case would be

$$\delta C_g(x,z_o) = C(x,z_o) - C_o. \qquad \text{[Eq. 3]}$$

An equivalent measure of δC_g can be made even in the presence of waves, however, if observations are made along a wave's surface. Measurements along the wavy surface, when adiabatic effects are removed, are equivalent to measurements made along its rest depth in the absence of motion. A surface of constant potential density moves with the waves. Making observations along the potential density surface with rest depth z_o gives glob-induced sound-speed fluctuations of

$$\delta C_g(x,z_o) = \hat{C}(x, \zeta(x)) - \hat{C}_o, \qquad \text{[Eq. 4]}$$

where $\hat{C}_o = C_o - \gamma z_o$.

The relative importance of salinity and temperature to glob-induced sound-speed fluctuations is seen as follows. By definition, along an iso-potential density surface

$$a\delta\hat{\theta} = b\delta S,$$

where in our case $a \approx 0.2 \times 10^{-3}(°C)^{-1}$, and $b \approx 0.8 \times 10^{-3}(‰)^{-1}$. Furthermore we may write

$$\delta C_g = \delta\hat{\theta}(\partial C/\partial\hat{\theta}) + \delta S(\partial C/\partial S),$$

The ratio of saline-induced to thermally-induced sound-speed fluctuations along the isopycnal is then

$$c = \frac{\delta S(\partial C/\partial S)}{\delta\hat{\theta}(\partial C/\partial\hat{\theta})} = \frac{a\beta}{b\alpha}, \qquad \text{[Eq. 5]}$$

where, for this case, $\alpha = C^{-1}(\partial C/\partial\hat{\theta}) = 2.5 \times 10^{-3}(°C)^{-1}$ and $\beta = C^{-1}(\partial C/\partial S) = 7.7 \times 10^{-4}(‰)^{-1}$, giving $c = 0.08$.

Case 3 — waves and globs

This is the total sound-speed variability one observes along $z = z_o$ in the presence of both waves and globs, which is simply

$$\delta C(x,z_o) = C(x,z_o) - C_o \qquad \text{[Eq. 6]}$$

3 ANALYSIS AND RESULTS

The data series $\zeta(x)$, $\hat{C}[x, \zeta(x)]$, and $\delta C(x,z_o)$, allowed examination of the records for total sound-speed variability and for the separate contributions due to waves and globs. The $\zeta(x)$ series was obtained by finding the elevation of a particular iso-potential density surface on every upward movement of the TOB, or roughly every 100 m along the ship's track. These series were then resampled at an even 100 m sampling length using linear interpolation. At each resulting point $(x, \zeta(x))$, $\hat{C}$ was determined*, yielding the second series of interest. Finally $C(x,z_o)$ was found at the same horizontal distances along the constant depth $z = z_o$. Using these variables determined from the measurements, and Eqs. 2, 4, and 6, the additional series $\delta C_w(x,z_o)$, $\delta C_g(x,z_o)$, and $\delta C(x,z_o)$ were formed for each segment of the tow pattern shown in Fig. 2. Examples of the data series are given in Fig. 6. They are from tow segment 3, which appears qualitatively to be in an area with a typical level of activity. These series were then multiplied by C_o^{-1} to give series of fractional sound-speed fluctuations.

3.1 The Spectra

The series are not stationary for spectral computations, so they were pre-whitened and the spectra later adjusted in order to compute the curves shown in Fig. 7**.

We see that at all wavelengths, the total fractional variability ($\delta C/C$) was approximately equal to ($\delta C_w/C$). At wavelengths less than 5 km, variability due to waves exceeded that due to globs by roughly a factor of 2. Variability due to globs decreased somewhat faster with wave number than did that due to waves, but they both varied approximately as k_H^{-2}. This was expected for ($\delta C_w/C$), as demonstrated in the next section.

---

* *Both $\hat{C}$ and C were computed by using equations from [6]. When calculating $\hat{C}$, z is set equal to zero and temperature is replaced by potential temperature.*

** *The high wavenumber portions of the observed spectra are somewhat suspect due to vertical filtering (see App. A).*

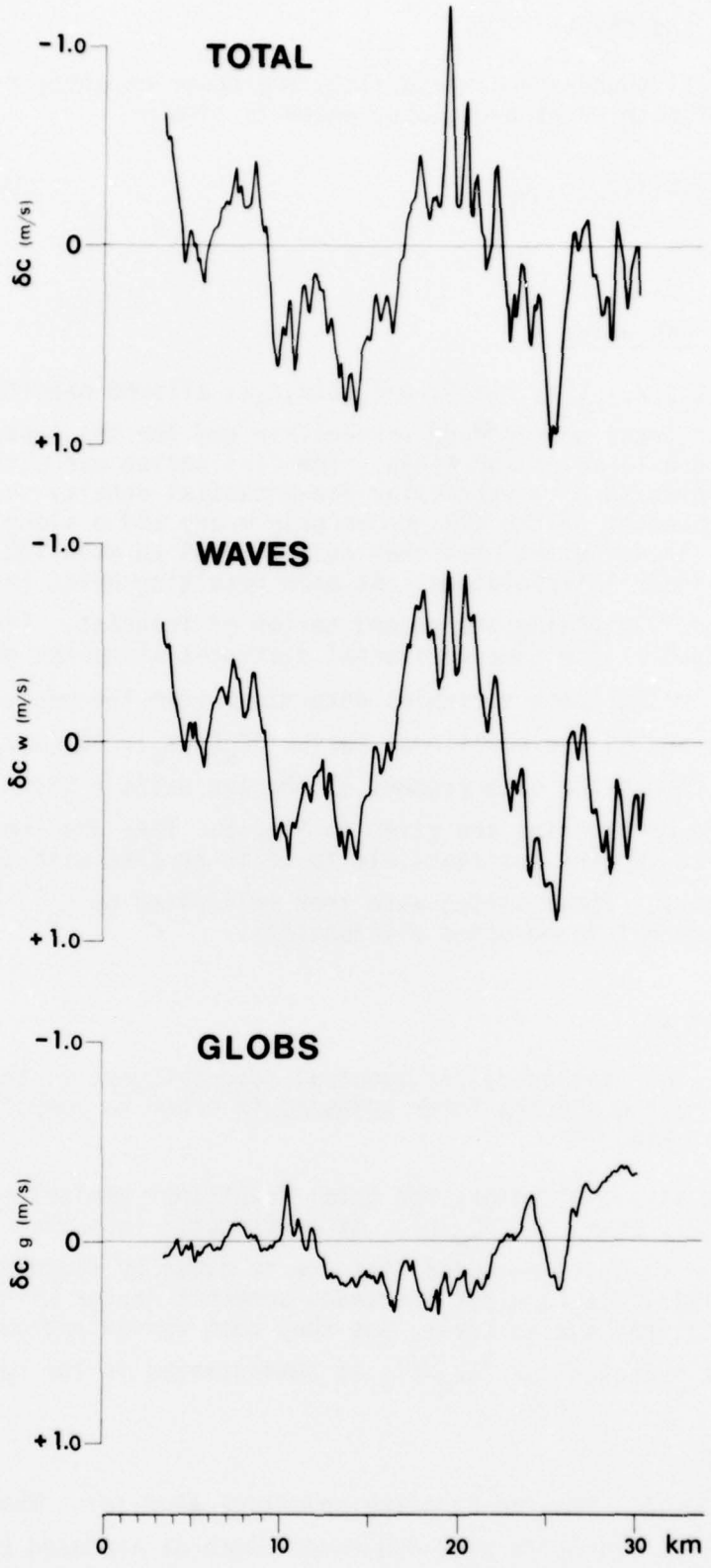

FIG. 6 EXAMPLES OF THE FLUCTUATIONS IN SOUND SPEED (δC) ALONG z = 145 m, AND THE FLUCTUATIONS IN SOUND SPEED DUE TO WAVES (δC_w) AND GLOBS (δC_g) ALONG THE SAME PATH. DATA ARE FROM A PORTION OF TOW SEGMENT 3

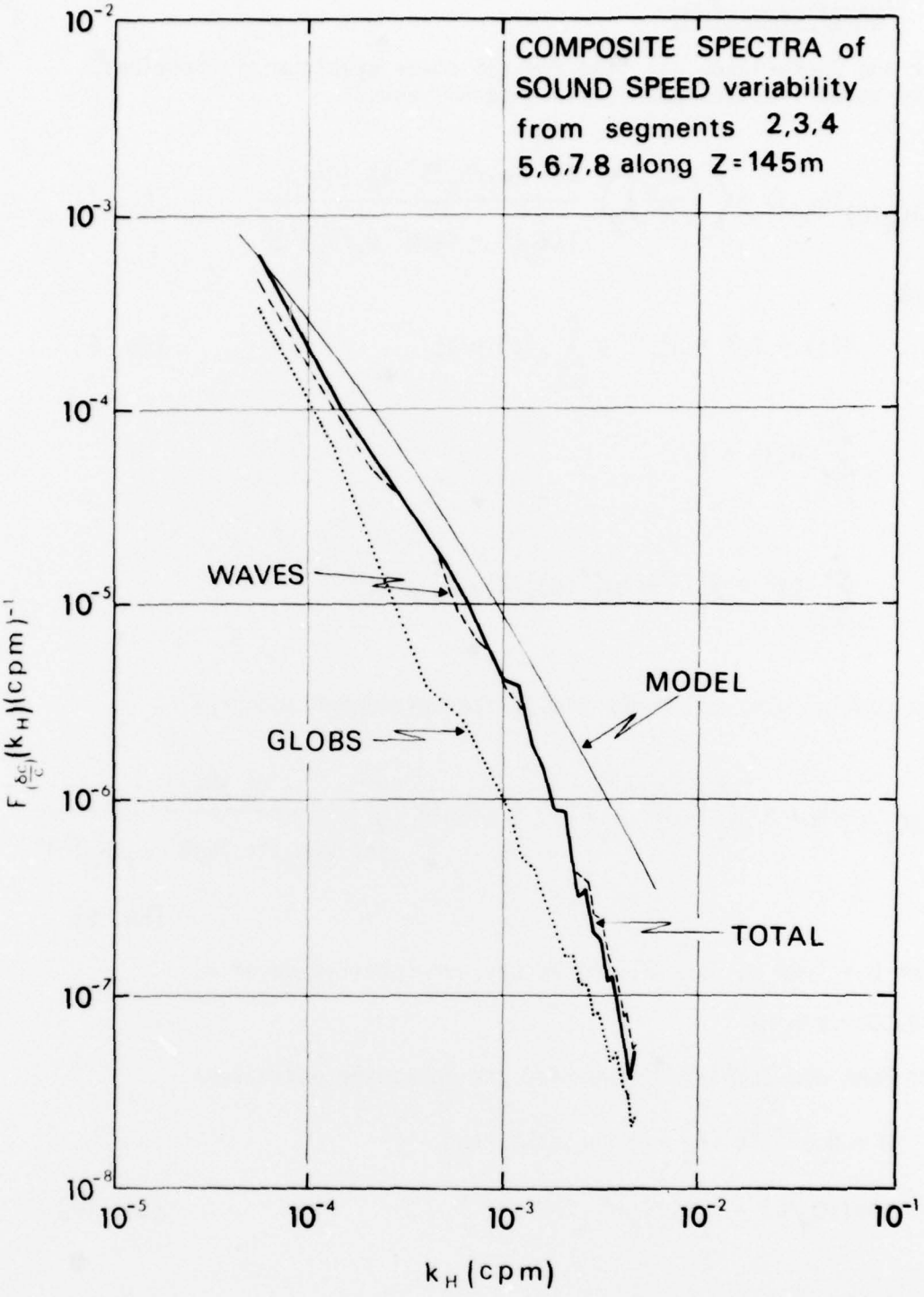

FIG. 7 WAVENUMBER SPECTRA OF THE TOTAL FRACTIONAL SOUND-SPEED FLUCTUATIONS ($\delta C/C$) ALONG z = 145 m, AND THE SPECTRA OF THE FRACTIONAL SOUND-SPEED FLUCTUATIONS DUE TO WAVES ($\delta C_w/C$) AND GLOBS ($\delta C_g/C$) OVER THE SAME PATHS. SPECTRAL DEGREES OF FREEDOM RANGE FROM 12 to 96. MODEL ESTIMATED SPECTRUM IS FROM MUNK & ZACHARIASEN [1]

3.2 Model Comparison

Munk and Zachariasen *[1]* find for the power spectrum of fractional sound-speed fluctuations due to internal waves*

$$F_{(\delta C_w/C)}(k_H,j) = \left\langle \left(\frac{\delta C_w}{C}\right)^2 \right\rangle \frac{2\pi^{-1}(\omega_i/N_o)B^{-1}k_H^2\, jH(j)}{[(k_H)^2 + (\tfrac{1}{2}jB^{-1}\omega_i/N_o)^2]^2} \qquad \text{[Eq. 7]}$$

where

$$H(j) = (j^2 + j_*^2)^{-1} \Big/ \sum_{j=1}^{\infty} (j^2 + j_*^2)^{-1}, \qquad \text{[Eq. 8]}$$

$$\sum_{j=1}^{\infty} H(j) = 1,$$

$$\sum_{j=1}^{\infty} (j^2 + j_*^2)^{-1} \approx \tfrac{1}{2}j_*^{-2}(\pi j_* - 1),\ j_* \geq 1.$$

Then summing over all modes yields the wavenumber spectrum

$$F_{(\delta C_w/C)}(k_H) = \left\langle \left(\frac{\delta C_w}{C}\right)^2 \right\rangle 2\pi^{-1}(\omega_i/N_o)B^{-1} \sum_{j=1}^{\infty} \frac{k_H^2\, jH(j)}{[(k_H)^2 + (\tfrac{1}{2}jB^{-1}\omega_i/N_o)^2]^2} \qquad \text{[Eq. 9]}$$

where B = 1000 m, $j_* = 3$, and we use our local value of ω_i (= 0.05 cycle/h).

From Munk and Zachariasen we make the following estimates:

$$N = N_o e^{-z/B};\ (N_o = 3 \text{ cycle/h}), \text{ and}$$

$$\text{rms}(\delta C_w/C) = \text{rms}(\delta C_w/C)_o (N/N_o)^{3/2} \qquad \text{[Eq. 10]}$$

---

*Our notation is slightly different from theirs. We use cyclical rather than circular wavenumbers for ease of comparison with the observed data.

with

$$\mathrm{rms}(\delta C_w/C)_o = (3.0 \times 10^{-6})\ \mu N_o^2\ \mathrm{rms}(\zeta_o) g^{-1}; \qquad \text{[Eq. 11]}$$

$\mathrm{rms}(\zeta_o) = 7.3$ m from *[5]* and

$$\mu = (\alpha/a)\ s(T_u). \qquad \text{[Eq. 12]}$$

In Eq. 12, $s = (1 + cT_u)$, where c is as defined previously (Eq. 5), and where the Turner number is

$$T_u = (b\ \frac{\partial S}{\partial z})\ /\ (a\ \frac{\partial \theta}{\partial z}). \qquad \text{[Eq. 13]}$$

Our gradients are typically $\frac{\partial S}{\partial z} = -2.2 \times 10^{-3} (‰) m^{-1}$, and $\frac{\partial \theta}{\partial z} = -1.4 \times 10^{-2} (°C) m^{-1}$, yielding $T_u = 0.63$, and $s = 2.8$.

From Eqs. 12, 11, 10, we calculate the model estimates $\mu = 22.0$; $\mathrm{rms}(\delta C_w/C)_o = 4.5 \times 10^{-4}$; and $\mathrm{rms}(\delta C_w/C) = 3.6 \times 10^{-4}$. The estimated mean squared value from the model is then

$$\left\langle \left(\frac{\delta C_w}{C} \right)^2 \right\rangle = 1.3 \times 10^{-7}$$

Replacing this in Eq. 9 gives us the Munk & Zachariasen model spectrum of internal-wave-induced fractional sound-speed fluctuations shown in Fig. 7. It is to be compared to the spectrum of observed wave-induced fluctuations, with which it agrees remarkably well.

3.3 Coherence Scales

To the extent that the Munk & Zachariasen model represents the Gulf of Cadiz environment, we may further use it to estimate the local horizontal (L_H) and vertical (L_V) coherence scales. The model gives

$$L_H = \frac{\pi (N_o/\omega_i) B}{8 j_* [\log_e (N/\omega_i) - 1/2]} = 2.2 \text{ km}, \qquad \text{[Eq. 14]}$$

and

$$L_v = \frac{B N_o / N}{(\pi j_*) - 1} = 0.14 \text{ km}. \qquad \text{[Eq. 15]}$$

These scales are z-dependent throughout N(z). The effect of globs will make the actual coherence distances somewhat less than these, and the above values should probably be viewed as upper limits.

3.4 The Nearshore Region

Spectra of sound-speed fluctuations along the individual tow segments were all more or less alike, with one exception. Measurements parallel to the bottom contours in the shallow (500 m) region traversed by track 8 (Fig. 2) were markedly quieter than the others. An example of the track 8 data is shown in Fig. 4. The spectrum of fluctuations from this path is compared in Fig. 8 with the overall spectrum from all paths. We see that sound-speed fluctuations along segment 8 are about a factor of 5 lower across nearly the whole spectrum, reflecting the fact that both glob and internal wave activities were low along the path. This is thought to be due primarily to anisotropy of the wave field in this shoaling water region, with wave crests aligned more parallel to the coast than perpendicular to it. If so, it is likely to be a general result that in the nearshore region sound-speed fluctuations parallel to the coast will be less than fluctuations along paths normal to the coast.

CONCLUSIONS

Sound-speed fluctuations have been examined by repeatedly profiling temperature, conductivity, and depth over long tow paths. The sound-speed variability due to internal waves conveniently separates from that due to inhomogeneities, revealing that even in an area of complex structure, internal waves are the leading cause of sound-speed fluctuations. At very low wavenumbers ($<10^{-4}$ cycle/m), variability due to globs nearly equaled that due to waves only, whereas at higher wavenumbers they contributed only about one fifth as much variability as waves.

The Munk & Zachariasen model estimate of wave-induced fluctuations agrees very well with these data, and allows the further computation of local coherence lengths.

We find a directional dependence of variability near the coast. Fluctuations were less by a factor of five looking along the coast than looking normal to it. We think it may be a general result that in shoaling areas sound-speed fluctuations measured parallel to the shore are less than those measured at right angles to the shore.

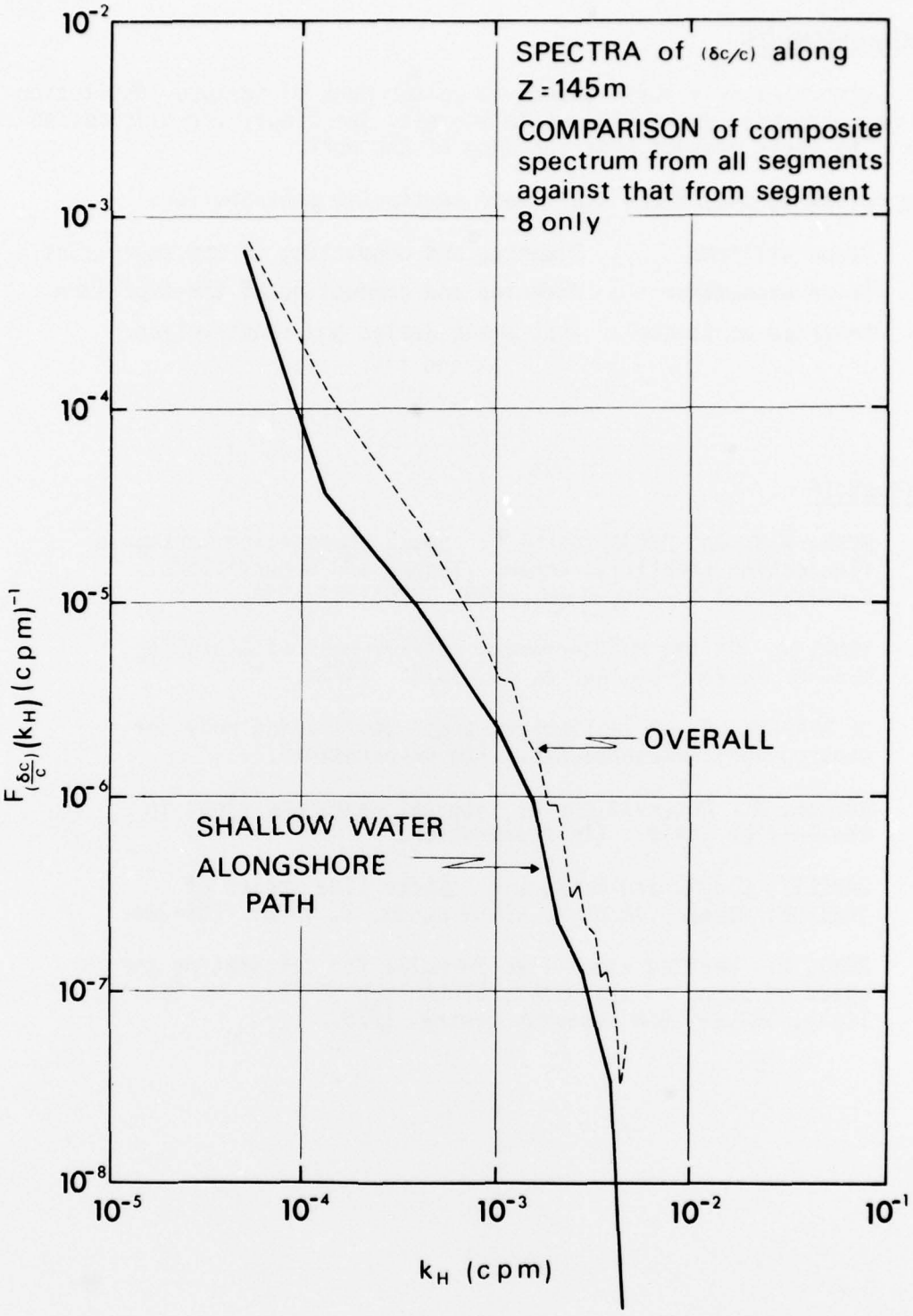

FIG. 8 SPECTRUM OF FRACTIONAL SOUND SPEED FLUCTUATIONS ALONG TOW TRACK 8 (shallow water alongshore path) COMPARED WITH OVERALL SPECTRUM FROM ALL PATHS. DEGREES OF FREEDOM ON OVERALL SPECTRUM RANGE FROM 12 to 96, AND ON SEGMENT 8 SPECTRUM FROM 8 to 30

ACKNOWLEDGMENTS

The authors express their thanks to Walter Munk of Scripps Institution of Oceanography, University of California, San Diego, for discussions basic to their present understanding of the work.

The following SACLANTCEN staff made particular contributions:

Bruce Williams : Planning and conducting of the experiment.

Brian Wannemaker : Planning and conducting of the experiment.

Federico de Strobel: Instrument design and construction.

REFERENCES

1. MUNK, W.H. and ZACHARIASEN, F. Sound propagation through a fluctuating stratified ocean: Theory and observations. *J Acoustical Society America* 59, 1976: 818-838.

2. ZENK, W. On the Mediterranean outflow west of Gibraltar, *Meteor. Forsch. Ergebn.* A, 16, 1975: 24-34.

3. DE STROBEL, F. A lightweight towed oscillating body for oceanographic measurements. (In preparation).

4. CAIRNS, J. Observations of internal waves and globs in the Gulf of Cadiz. (In preparation).

5. GARRETT, C.J.R. and MUNK, W.H. Space time scales of internal waves. *Geophys. Fluid Dynam.* 2, 1972: 255-264.

6. ROSS, D. Revised simplified formulae for calculating the speed of sound in sea water, SACLANTCEN SM-107. La Spezia, Italy, SACLANT ASW Research Centre, 1978.

APPENDIX A

There are some inherent problems in making measurements from a pitching ship using sensors with finite and diverse time responses. These are especially bothersome when information from multiple sensors must be combined to calculate another variable such as density or sound speed. Pingree *[A.1]* gives a good description of the situation. A sensor lowered from an equilibrated position requires some time to notice it has moved. If lowered uniformly through a smooth gradient it eventually parallels the true trace but lags behind it. If its descent slows or stops, however, it will continue to equilibrate and its trace will curve over to join the true one. Alternate slowing and speeding of the descent results in a wobbly trace that lags the true smooth trace; the effect is reversed on the ascent. In principle one can remove these effects if the sensor has sufficiently well known and well behaved characteristics. But in practice their removal is quite difficult, especially as they effect, say, computed density.

Wiggles were found in our density profiles with a regularity of about once each six seconds (or each six metres vertically). The power spectrum of vertical sensor speed derived from the first difference record of the pressure sensor was also sharply peaked at 1/6 Hz, indicating the pitching response of the ship to the encounter of the ocean waves.

We have minimized these effects in our data at the expense of vertical resolution by filtering all of the data with a filter whose vertical high wavenumber cutoff is 0.07 cycle/min (14 m vertical scale). To compensate for the phase shift induced by its longer constant, the temperature record is then shifted back in time by 0.34 s ($\approx$1 time constant) relative to conductivity and depth. This time shift was determined empirically by minimizing the small-scale variance in computed density profiles. All the variables including the calculated density and sound speed are then very well behaved, but we are constrained to look at features with large vertical scales.

REFERENCE

A.1 PINGREE, R.D. Regularly spaced instrumental temperature and salinity structure. *Deep Sea Research* 18, 1971: 841-844.